

---

# Hypersolvers: Toward Fast Continuous-Depth Models

---

**Michael Poli\***  
KAIST  
poli\_m@kaist.ac.kr

**Stefano Massaroli\***  
The University of Tokyo  
massaroli@robot.t.u-tokyo.ac.jp

**Atsushi Yamashita**  
The University of Tokyo  
yamashita@robot.t.u-tokyo.ac.jp

**Hajime Asama**  
The University of Tokyo  
asama@robot.t.u-tokyo.ac.jp

**Jinkyoo Park**  
KAIST  
jinkyoo.park@kaist.ac.kr

## Abstract

The infinite-depth paradigm pioneered by Neural ODEs has launched a renaissance in the search for novel dynamical system-inspired deep learning primitives; however, their utilization in problems of non-trivial size has often proved impossible due to poor computational scalability. This work paves the way for scalable Neural ODEs with *time-to-prediction* comparable to traditional discrete networks. We introduce *hypersolvers*, neural networks designed to solve ODEs with low overhead and theoretical guarantees on accuracy. The synergistic combination of hypersolvers and Neural ODEs allows for cheap inference and unlocks a new frontier for practical application of continuous-depth models. Experimental evaluations on standard benchmarks, such as sampling for *continuous normalizing flows*, reveal consistent pareto efficiency over classical numerical methods.

## 1 Introduction

The framework of *neural ordinary differential equations* (Neural ODEs) (Chen et al., 2018; Rubanova et al., 2019) has reinvigorated research in continuous deep learning (Zhang et al., 2014), offering new system-theoretic perspectives on neural network architecture design (Greydanus et al., 2019; Bai et al., 2019; Poli et al., 2019; Cranmer et al., 2020) and generative modeling (Grathwohl et al., 2018; Yang et al., 2019). Despite the successes, Neural ODEs have been met with skepticism, as these models are often slow in both training and inference due to heavy numerical solver overheads. These issues are further exacerbated by applications which require extremely accurate numerical solutions to the differential equations, such as physics-inspired neural networks (Raissi et al., 2019) and continuous normalizing flows (CNFs) (Chen et al., 2018).

Common knowledge within the field is that these models appear too slow in their current form for meaningful large-scale or embedded applications. Several attempts have been made to either directly or indirectly address some of these limitations, such as redefining the forward pass as a root finding problem (Bai et al., 2019), introducing *ad hoc* regularization terms (Finlay et al., 2020; Massaroli et al., 2020a) and augmenting the state to reduce stiffness of the solutions (Dupont et al., 2019; Massaroli et al., 2020b). Unfortunately, these approaches either give up on the Neural ODE formulation altogether, do not reduce computation overhead sufficiently or introduce additional memory requirements.

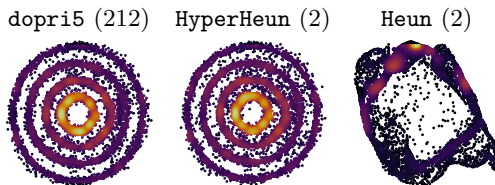


Figure 1: Hypersolvers for density estimation via *continuous normalizing flows*: dopri5 inference accuracy is achieved with 100x speedup and memory efficiency.

---

\*Equal contribution

Although there is no shortage of works utilizing Neural ODEs in forecasting tasks (Yildiz et al., 2019; Jia and Benson, 2019; Kidger et al., 2020), current state-of-the-art is limited to offline applications with no constraints on inference time. In particular, high-potential application domains for Neural ODEs such as control and prediction often deal with tight requirements on inference speed and computation e.g robotics (Hester, 2013) that are not currently within reach. For example, a generic state-of-the-art convolutional Neural ODE takes at least an order of magnitude<sup>2</sup> longer to infer the label of a *single* MNIST image. This inefficiency results in inference passes far too slow for real-time applications.

Method	NFEs	Local Error
$p$ -th order solver	$\mathcal{O}(pK)$	$\mathcal{O}(\epsilon^{p+1})$
adaptive-step solver	–	$\mathcal{O}(\bar{\epsilon}^{p+1})$
Euler hypersolver	$\mathcal{O}(K)$	$\mathcal{O}(\delta\epsilon^2)$
$p$ -th order hypersolver	$\mathcal{O}(pK)$	$\mathcal{O}(\delta\epsilon^{p+1})$

Figure 2: Asymptotic complexity comparison. Number of function evaluations (NFEs) needed to compute  $K$  solver’s steps.  $\epsilon$  is the step size,  $\bar{\epsilon}$  is the max step size of adaptive solvers,  $\delta \ll 1$  is correlated to the hypersolver training results.

The interplay between Neural ODEs and numerical solvers has largely been overlooked as research on model variants has been predominant, often treating solver choice as a simple hyper-parameter to be tuned based on empirical observations. Here, we argue for the importance of computational scalability outside of specific Neural ODE architectural modifications, and highlight the synergistic combination of model-solver to be a likely candidate for unlocking the full potential of continuous-depth models. Namely, this work attempts to alleviate computational overheads by introducing the paradigm of Neural ODE *hypersolvers*; these auxiliary, shallow neural networks are trained to

solve the initial value problem (IVP) emerging from the forward pass of continuous-depth models. Hypersolvers improve on the computation-correctness trade-off provided by traditional numerical solvers, enabling fast and arbitrarily accurate solutions during inference.

**Pareto efficiency** The trade-off between solution accuracy and computation is one of the oldest and best-studied topics in the numerics literature (Butcher, 2016) and was mentioned in the seminal work (Chen et al., 2018) as a feature of continuous models. Traditional methods shift additional compute resources into improved accuracy via higher-order adaptive-step numerical methods (Prince and Dormand, 1981). For the most part, the computation-accuracy pareto front determined by traditional methods has been treated as optimal, allowing practitioners and researchers its traversal with different solver choices. We provide theoretical and practical results in support of the pareto efficiency of hypersolvers introduced by Fig. 1 compared to traditional methods.

**Inference speed** By leveraging Hypersolved Neural ODEs, we obtain significant speedups on common benchmarks for continuous-depth models. In image classification tasks, inference is sped up by *at least* one order of magnitude. Additionally, the proposed approach is capable of solving *continuous normalizing flow* (CNF) (Chen et al., 2018; Grathwohl et al., 2018) sampling in few steps with little-to-no degradation of the sample quality as shown in Fig. 1.

**Model-solver synergy** Moving beyond computational advantages at inference time, the proposed framework is compatible with *continual learning* (Parisi et al., 2019) or *adversarial learning* (Ganin et al., 2016) techniques where model and hypersolver are co-designed and jointly optimized. Sec. 6 provides an overview and a proof of concept of this peculiar interplay.

## 2 Background: Continuous-Depth Models

We start by introducing necessary background on Neural ODE and numerical integration methods.

**Neural ODEs** In this work, we consider the following general data-controlled (Massaroli et al., 2020b) Neural ODE formulation

$$\begin{cases} \dot{\mathbf{z}} = f_{\theta(s)}(\mathbf{x}, s, \mathbf{z}(s)) \\ \mathbf{z}(0) = h_x(\mathbf{x}) \\ \hat{\mathbf{y}}(s) = h_y(\mathbf{z}(s)) \end{cases} \quad s \in \mathcal{S} \quad (1)$$

<sup>2</sup>Compared with an equivalent-performance ResNet.

with input  $\mathbf{x} \in \mathbb{R}^{n_x}$ , output  $\hat{\mathbf{y}} \in \mathbb{R}^{n_y}$ , *hidden* state  $\mathbf{z} \in \mathbb{R}^{n_z}$  and  $\mathcal{S}$  is a compact subset of  $\mathbb{R}$ . Here  $f_{\theta(s)}$  is a neural network, parametrized by  $\theta(s)$  in some functional space. We equip the Neural ODE with input and output mappings  $h_x : \mathbb{R}^{n_x} \rightarrow \mathbb{R}^{n_z}$ ,  $h_y : \mathbb{R}^{n_z} \rightarrow \mathbb{R}^{n_y}$  which are kept linear as to avoid a collapse of the dynamics into a non-necessary map as discussed in (Massaroli et al., 2020b).

**Solving the ODE** Without any loss of generality, let  $\mathcal{S} := [0, S]$  ( $S \in \mathbb{R}^+$ ). The inference of Neural ODEs is carried out by solving the *initial value problem* (IVP) (1), i.e.

$$\hat{\mathbf{y}}(S) = h_y \left( h_x(\mathbf{x}) + \int_{\mathcal{S}} f_{\theta(\tau)}(\mathbf{x}, \tau, \mathbf{z}(\tau)) d\tau \right)$$

Due to the nonlinearities of  $f_{\theta(s)}$ , this solution cannot be defined in closed-form and, thus, a numerical solution should be obtained by iterating some predetermined ODE solver. Let us divide  $\mathcal{S}$  in  $K$  equally-spaced intervals  $[s_k, s_{k+1}]$  such that for all  $k \in \mathbb{N}_{<K}$   $s_{k+1} - s_k = S/K := \epsilon \in \mathbb{R}^+$ . The numerical approximation of the IVP solution in  $\mathcal{S}$  can be computed by iterating

$$\begin{cases} \mathbf{z}_{k+1} = \mathbf{z}_k + \epsilon \psi(\mathbf{x}, s_k, \mathbf{z}_k) \\ \mathbf{z}_0 = h_x(\mathbf{x}) \\ \hat{\mathbf{y}}_k = h_y(\mathbf{z}_k) \end{cases} \quad k = 0, 1, \dots, K-1 \quad (2)$$

where  $\psi$  is a function performing the state update.

**Numerical methods** Diverse ODE solvers differ in how this map  $\psi$  is constructed<sup>3</sup>. In example, the Euler method is realized by setting  $\psi(\mathbf{x}, s_k, \mathbf{z}_k) := f_{\theta(s_k)}(\mathbf{x}, s_k, \mathbf{z}_k)$ . Note that, *higher-order* solvers compute  $\psi(\mathbf{x}, s_k, \mathbf{z}_k)$  iteratively in  $p$  steps where  $p$  denotes the order of the solver. For example, in a  $p$ -th order Runge-Kutta (RK) (Runge, 1895) method  $\psi$  is computed as

$$\begin{aligned} \mathbf{r}_i &= f_{\theta(s_k)}(\mathbf{x}, s_k + \mathbf{c}_i \epsilon, \mathbf{z}_k + \tilde{\mathbf{z}}_k^i) \quad i = 1, \dots, p \\ \tilde{\mathbf{z}}_k^i &= \epsilon \sum_{j=1}^p \mathbf{a}_{ij} \mathbf{r}_j \quad i = 1, \dots, p \\ \psi &= \sum_{j=1}^p \mathbf{b}_j \mathbf{r}_j \end{aligned}$$

where  $\mathbf{a} \in \mathbb{R}^{p \times p}$ ,  $\mathbf{b} \in \mathbb{R}^p$ ,  $\mathbf{c} \in \mathbb{R}^p$  fully characterize the method. Hence, the integration of a neural ODE in  $\mathcal{S}$  with a RK solver is  $\mathcal{O}(pK)$  in memory efficiency and time complexity. On the other hand, *adaptive-step* solvers, e.g. the popular Dormand-Prince 5(4) (dopri5) have no explicit upper bounds in memory and time efficiency. This is especially critical as in many practical applications, a requirement for maximum memory consumption and/or inference time must be satisfied.

**Common metrics** In classic numerical analysis, two type of metrics are often defined, i.e. the *local truncation error*  $e_k$

$$e_k := \|\mathbf{z}(s_{k+1}) - \mathbf{z}(s_k) - \epsilon \psi(\mathbf{x}, s_k, \mathbf{z}(s_k))\|_2,$$

representing the error accumulated in a single step, and the *global truncation error*  $\mathcal{E}_k$  is

$$\mathcal{E}_k = \|\mathbf{z}(s_k) - \mathbf{z}_k\|_2,$$

i.e. the error accumulated in the first  $k$  steps. Note that for a  $p$ -th order solver  $e_k = \mathcal{O}(\epsilon^{p+1})$  and  $\mathcal{E}_k = \mathcal{O}(\epsilon^p)$  (Butcher, 2016).

### 3 Hypersolvers for Neural ODEs

The core idea behind hypersolvers is to introduce an additional neural network  $g_\omega$  to approximate the higher-order terms of a given solver, greatly increasing its accuracy while preserving the computational and memory efficiency. The simplest instance of *Hypersolved* Neural ODEs is based on Euler scheme:

$$\begin{cases} \mathbf{z}_{k+1} = \mathbf{z}_k + \epsilon f_{\theta(s_k)}(\mathbf{x}, s_k, \mathbf{z}_k) + \epsilon^2 g_\omega(\epsilon, \mathbf{x}, s_k, \mathbf{z}_k) \\ \mathbf{z}_0 = h_x(\mathbf{x}) \\ \hat{\mathbf{y}}_k = h_y(\mathbf{z}_k) \end{cases} \quad k = 0, 1, \dots, K-1 \quad (3)$$

<sup>3</sup>Numerical solvers which obey to (2) are called *single-step* or *explicit* solvers

where  $g_\omega$  is a neural network approximating the second-order term of the Euler method. The derivation of the *Euler hypersolver* comes naturally from the following. Let  $\mathbf{z}(s_k)$  be the true solution of (1) at  $s_k \in \mathcal{S}$  and let  $\epsilon > 0$  such that  $s_k + \epsilon \in \mathcal{S}$ . From the Taylor expansion of the solution around  $s_k$ , i.e.

$$\begin{aligned} \mathbf{z}(s_k + \epsilon) &= \mathbf{z}(s_k) + \epsilon \dot{\mathbf{z}}(s_k) + \frac{1}{2} \epsilon^2 \ddot{\mathbf{z}}(s_k) + \mathcal{O}(\epsilon^3) \\ &\approx \mathbf{z}(s_k) + \epsilon f_\theta(\mathbf{x}, s_k, \mathbf{z}(s_k)) \end{aligned}$$

we deduce that the classic Euler scheme corresponds to the first-order truncation of the above. The Euler hypersolver, instead, aims at approximating the second-order term, reducing the local truncation error of the overall scheme, while avoiding to compute and store further evaluations of  $f_\theta(s)$ , as required by higher order schemes, e.g. RK methods.

**General formulation** Note that, a general formulation of Hypersolved Neural ODEs can be obtained directly from (2). If we assume  $\psi$  to be the update step of a  $p$ -th order solver, then the general  $p$ -th order Hypersolved Neural ODE is defined as

$$\begin{cases} \mathbf{z}_{k+1} = \mathbf{z}_k + \epsilon \psi(\mathbf{x}, s_k, \mathbf{z}_k) + \epsilon^{p+1} g_\omega(\epsilon, \mathbf{x}, s_k, \mathbf{z}_k) \\ \mathbf{z}_0 = h_x(\mathbf{x}) \\ \hat{\mathbf{y}}_k = h_y(\mathbf{z}_k) \end{cases} \quad k = 0, 1, \dots, K-1 \quad (4)$$

**Software implementation** We have implemented “hyper” versions of common low-order ODE solvers designed for compatibility with the `torchdiffeq` (Chen et al., 2018) library. To facilitate reproducibility, we provide in the Appendix a short PyTorch (Paszke et al., 2017) code snippet for Euler and Heun hypersolver variants. The full implementation will be released after the review phase and is included in the submission.

### 3.1 Training Hypersolvers

Assume to have available the *exact* solution of the Neural ODE evaluated at the mesh points  $s_k$ , practically obtained through an adaptive-step solver set up with low tolerances. With these solution checkpoints we construct the training set for the DE solver with tuples:

$$\{(s_k, \mathbf{z}(s_k))\}_{k \in \mathbb{N}_{\leq K}}$$

According to the introduced metrics  $e_k$  and  $\mathcal{E}_k$ , we introduce two types of loss functions aimed at improving each of the metrics.

**Residual fitting** We first start by defining the *residual* of the solver (2)

$$\mathcal{R}(s_k, \mathbf{z}(s_k), \mathbf{z}(s_{k+1})) = \frac{1}{\epsilon^{p+1}} [\mathbf{z}(s_{k+1}) - \mathbf{z}(s_k) - \epsilon \psi(\mathbf{x}, s_k, \mathbf{z}(s_k))] \quad (5)$$

which correspond to a scaled local truncation error without the neural correction term  $g_\omega$ . Then, we can consider a loss measuring the discrepancy between the residual terms and the output of  $g_\omega$ :

$$\ell = \frac{1}{K} \sum_{k=0}^{K-1} \|\mathcal{R}(s_k, \mathbf{z}(s_k), \mathbf{z}(s_{k+1})) - g_\theta(\epsilon, \mathbf{x}, s_k, \mathbf{z}(s_k))\|_2$$

If the hypersolver is trained to minimize  $\ell_{\text{local}}$ , the following holds:

**Theorem 1** (Hypersolver’s Local Truncation Error). *If  $g_\omega$  is a  $\mathcal{O}(\delta)$  approximator of  $\mathcal{R}$ , i.e.*

$$\forall k \in \mathbb{N}_{\leq K} \quad \|\mathcal{R}(s_k, \mathbf{z}(s_k), \mathbf{z}(s_{k+1})) - g_\theta(\epsilon, \mathbf{x}, s_k, \mathbf{z}(s_k))\|_2 \leq \mathcal{O}(\delta),$$

*then, the local truncation error  $e_k$  of the hypersolver is  $\mathcal{O}(\delta \epsilon^{p+1})$ .*

The proof and further theoretical insights are reported in the Appendix.

**Trajectory fitting** The second type of hypersolvers training aims at containing the global truncation error by minimizing the difference between the exact and approximated solutions in the whole depth domain  $\mathcal{S}$ , i.e.

$$L = \sum_{k=1}^K \|\mathbf{z}(s_k) - \mathbf{z}_k\|_2$$

It should be noted that *trajectory* and *residual fitting* can be combined into a single loss term, depending on the application.

## 4 Experimental Evaluation

The proposed model is evaluated on key benchmarks for Neural ODEs. First, we leverage hypersolver pareto efficiency to obtain large inference speedups in the *number of function evaluations* (NFEs) for image classification tasks. We then show how Hypersolved Neural ODEs can generate *continuous normalizing flow* (CNF) samples with a fraction of the NFEs required by the vanilla approach, without degradation of the recovered density.

### 4.1 Image Classification

Following the setup of (Dupont et al., 2019), we train convolutional Neural ODEs with input-layer augmentation (Massaroli et al., 2020b) on MNIST and CIFAR10 datasets using standard methods. Following this initial optimization step, 2-layer convolutional *Euler hypersolvers* (3) are trained by residual fitting (5) on 20 epochs of the training dataset with solution mesh length set to  $K = 10$ . As the ground-truth labels, we utilize the solutions obtained via `dopri5` with absolute and relative tolerances set to  $10^{-3}$  on the same data. The objective of this first task is to show that hypersolvers retain their pareto efficiency when applied in high-dimensional data regimes. Additional details on hyperparameter choice and architectures are provided as supplementary material.

**Solution accuracy** Figures 3 and 4 show the absolute error between `dopri5` and the hypersolver (top) and Euler at mesh grids points  $k = 1, \dots, 9$  summed across channels of a data sample. While inference speedups can also be obtained by utilization of low-order fixed-step solvers, this choice causes great performance degradation in solution accuracy. The hypersolvers, on the other hand, are able to accurately solve the MNIST and CIFAR10 Neural ODEs.

**Pareto comparison** We provide pareto plots of terminal *mean absolute percentage error* (MAPE) of the ODE solutions and average test classification accuracy loss of various solution methods compared to `dopri5`. As shown in Figures 3 and 4, the Euler hypersolver enjoys the best compromise between a minimization of the ODE solution error with a  $< 1\%$  effect on the test classification accuracy at around 10 NFEs. Interestingly, the hypersolver is able to generalize to different step sizes and in this particular instance is more pareto efficient than Euler and higher-order solvers (midpoint and RK4). CIFAR10 Neural ODE first-order hypersolvers provide similar pareto efficiency benefits, though as predicted by theoretical bounds, higher-order methods outperform them at higher NFEs.

We measure the inference speedup (in NFEs) of Hypersolved Neural ODEs with  $K = 10$  to be 10x compared to `dopri5` for a complete inference pass on the entire MNIST test set, with similar gains on CIFAR10. In practice, computation time speedups depend on both hardware and implementation overhead, though our measurements on a single Tesla V100 GPU are consistent with the above.

### 4.2 Lightweight FFJORD Sampling

We consider sampling in the FFJORD (Grathwohl et al., 2018) variant of *continuous normalizing flows* (Chen et al., 2018) as an additional task showcasing the hypersolving speed and accuracy.

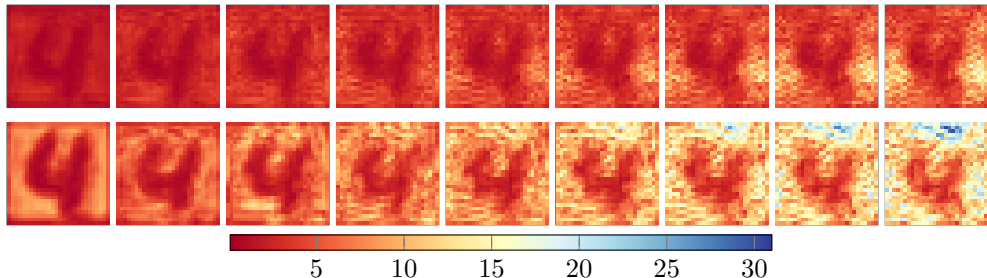


Figure 3: Absolute integration error propagation through the depth domain of the HyperEuler (above) and Euler (below) methods on MNIST data.

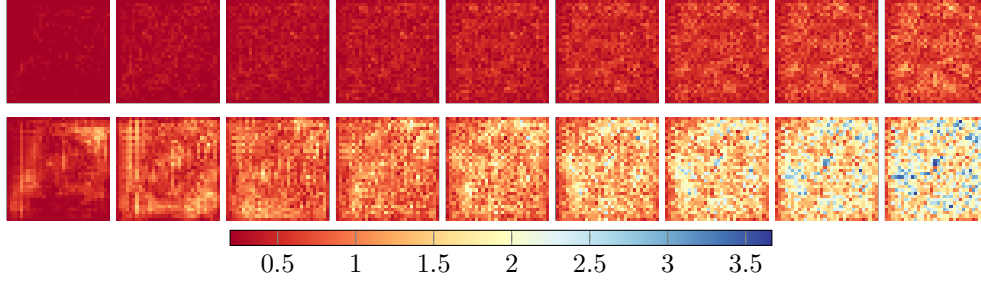


Figure 4: Absolute integration error propagation through the depth domain of the HyperEuler (above) and Euler (below) methods on CIFAR10 data.

**Density inspection** We train CNFs closely following the setup of Grathwohl et al. (2018). Then, we optimize two-layer, second-order Heun hypersolvers with the  $K = 2$  residuals obtained against dopri5 with absolute tolerance  $10^{-5}$  and relative tolerance  $10^{-5}$ . The striking result highlighted in Fig. 6 is that with as little as two NFEs, Hypersolved CNFs provide samples that are as accurate as those obtained through dopri5.

**Depth-reversibility** These experiments have also been designed to suggest applications of the hypersolver paradigm outside of the inference step. Indeed, the Heun method enjoys depth-reversibility (see Appendix) and its hypersolver analogue can thusly be trained on forward pass of the CNF. In this way, the same hypersolver can be used for both sample generation as well as density estimation, without additional fine-tuning.

## 5 Related Work

**Neural network solvers** There is a long line of research leveraging the universal approximation capabilities of neural networks for solving differential equations. A recurrent theme of the existing work (Lagaris et al., 1997, 1998; Li-ying et al., 2007; Li and Li, 2013; Mall and Chakraverty, 2013; Raissi et al., 2018; Qin et al., 2019) is direct utilization of noiseless analytical solutions and evaluations in low dimensional settings. Application specific attempts (Xing and McCue, 2010; Breen et al., 2019; Fang et al., 2020) provide empirical evidence in support of the earlier work, though the approximation task is still cast as a gradient-matching regression problem on noiseless labels. Deep neural network base solvers have also been used in the distributed parameters setting for PDEs (Han et al., 2018; Magill et al., 2018; Weinan and Yu, 2018; Raissi, 2018; Piscopo et al., 2019; Both

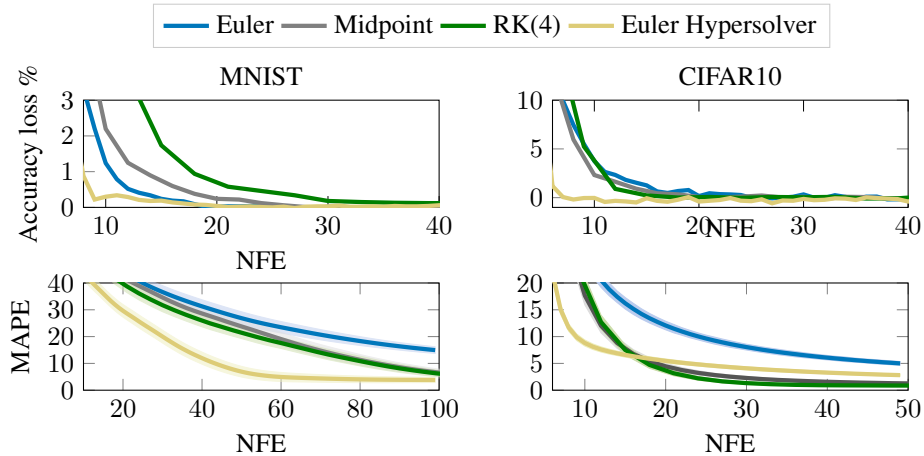


Figure 5: Test accuracy loss %-NFE and MAPE-NFE Pareto fronts of different ODE solvers on MNIST and CIFAR10 test sets. The HyperEuler always shows higher Pareto optimality for low function evaluations (NFEs).

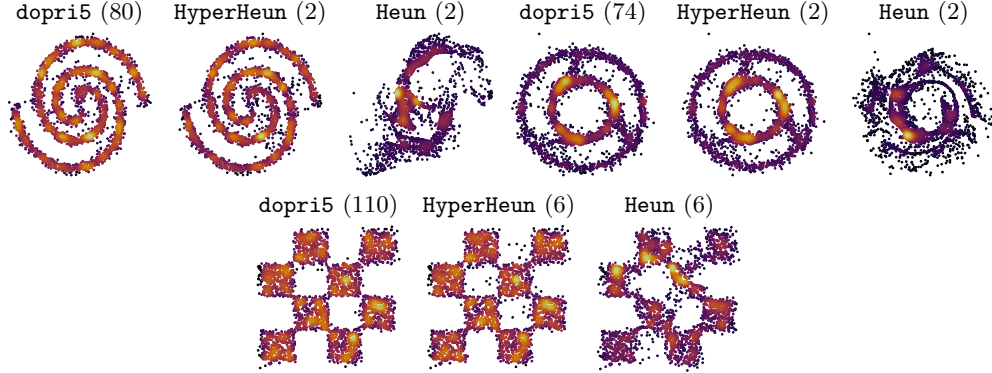


Figure 6: Reconstructed densities with continuous normalizing flows and Heun hypersolver HyperHeun. The inference accuracy of dopri5 is reached through the hypersolver with a significant speedup in terms of computation time and accuracy. Heun method fails to solve correctly the ODE with same NFEs of HyperHeun.

et al., 2019; Khoo and Ying, 2019; Winovich et al., 2019; Raissi et al., 2019). More recent advances involving symbolic regressions include (Winovich et al., 2019; Regazzoni et al., 2019; Long et al., 2019).

The hypersolver approach is different in several key aspects. To the best knowledge of the authors, this represents the first example where neural network solvers show both *consistent* and *significant* pareto efficiency improvements over traditional solvers in high-dimensional settings. The performance advantages are demonstrated in the absence of analytic solutions and are supported by theoretical guarantees, ultimately yielding large inference speedups of practical relevance for Neural ODEs.

**Multi-stage ResNets** After seminal research (Sonoda and Murata, 2017; Lu et al., 2017; Chang et al., 2017; Hauser and Ray, 2017; Chen et al., 2018) uncovered and strengthened the connection between ResNets and ODE discretizations, a variety of architecture and objective specific adjustments have been made to the vanilla formulation. The above allow, for example, to accommodate irregular observations in sequence data (Demeester, 2019) or inherit beneficial properties from the corresponding numerical methods (Zhu et al., 2018). Although these approaches share some structural similarities with the Hypersolved formulation (3), the objective is drastically different. Indeed, such models are optimized for task-specific metrics without concern about preserving ODE properties, or developing a synergistic connection between model and solver.

## 6 Discussion

We discuss the interplay of model-hypersolver beyond *inference* steps.

**Continual learning of Neural ODE dynamics** A particularly attractive formulation for the use of hypersolvers to speed up training of continuous-depth models involves *continual learning* (Parisi et al., 2019) of Neural ODE dynamics. Consider the problem of approximating the solution of a Neural ODE at training iteration  $t + 1$  having trained the hypersolver on flows generated by the Neural ODE  $f_{\theta_t(s)}(\mathbf{x}_t, s, \mathbf{z}(s))$  at the previous training step  $t$ . In contrast to many continual learning problems, this setting involves a certifiably smooth transition between tasks that is directly controlled by the learning rate  $\eta$ , leading to the following result

**Proposition 1** (Vector field training sensitivity). *Let the model parameters  $\theta_t(s)$  be updated according to the gradient-based optimizer step*

$$\theta_{t+1}(s) = \theta_t(s) + \eta \Gamma(\nabla_{\theta(s)} \mathcal{L}_t), \quad \eta > 0$$

*to minimize a loss function  $\mathcal{L}_t$  and let  $f_{\theta_t(s)}$  be Lipschitz w.r.t.  $\theta(s)$ . Then,*

$$\forall \mathbf{z} \in \mathbb{R}^{n_z}, \quad \|\Delta f_{\theta_t}(\mathbf{x}, s, \mathbf{z})\|_2 \leq \eta L_{\theta(s)} \|\Gamma(\nabla_{\theta(s)} \mathcal{L})\|_2$$

*being  $L_{\theta}$  the Lipschitz constant.*

Similar to recent advances in *natural language processing* (Howard and Ruder, 2018; Devlin et al., 2018), we envision pretraining and continual learning techniques for hypersolvers to play a fundamental part in the search for easy-to-train Neural ODEs. In particular, by leveraging the above result, it might be possible to constructively design a training procedure maximizing hypersolver reutilization across as many training iterations as possible.

**Adversarial and joint training** The interplay between hypersolver and Neural ODE lends itself to a formulation amenable to *adversarial training* (Ganin et al., 2016; Goodfellow et al., 2014). In the standard setting, numerical solvers already act as adversaries preserving the ODE solution accuracy at the cost of model expressivity. Taking this analogy further, we propose optimizing for adversarial loss terms in the form:

$$\min_{\omega} \max_{\theta} \sum_{k=0}^K \|\mathbf{z}_k - \bar{\mathbf{z}}_k\|_2 \quad (6)$$

where  $\bar{\mathbf{z}}_k$  is the solution at mesh point  $k$  given by an adaptive step solver. When used either during hypersolver pretraining or as a regularization term for the main task, the above gives rise to emerging behaviors in the dynamics  $f_{\theta(s)}$  which exploit solver weaknesses. We show one such example in Fig. 6, where optimizing purely for (6) teaches  $f_{\theta(s)}$  to exploit *stiffness* (Shampine, 2018) of the differential equation to increase the hypersolver solution error.

By learning to defend against such attempts,  $g_{\omega}$  enjoys improved robustness. In the Appendix we include additional details motivating the importance of stiffness in the context of hypersolvers.

Similarly, hypersolver and Neural ODE training can be carried out *jointly* during optimization for the main task, by mixing and matching loss terms appropriately. When the performance is deemed sufficient, Neural ODE training can continue at a quicker pace by utilizing the hypersolver instead.

**Hypersolver agents** Hypersolvers are trained on solution data that is cheap to generate. The framework results immediately compatible with classical and meta-*reinforcement learning* (RL) (Gupta et al., 2018), offering a plethora of methods for hypersolver *agents* capable of generalizing across different Neural ODE dynamics.

## 7 Conclusion

Computational overheads represent a great obstacle for the utilization of continuous-depth models in large scale or real-time applications. In this work we alleviate these limitations by introducing the paradigm of *hypersolvers*, neural networks trained to solve Neural ODEs accurately and with low overhead. The synergistic combination of Hypersolvers and Neural ODEs enjoys large speedups during inference steps of standard benchmarks of continuous-depth models, allowing accurate sampling from *continuous normalizing flows* (CNFs) in as little as 2 *number of function evaluations* (NFEs). Finally, the hypersolver framework is shown to be compatible with *continual learning* or *adversarial training* techniques to affect Neural ODE training as well.

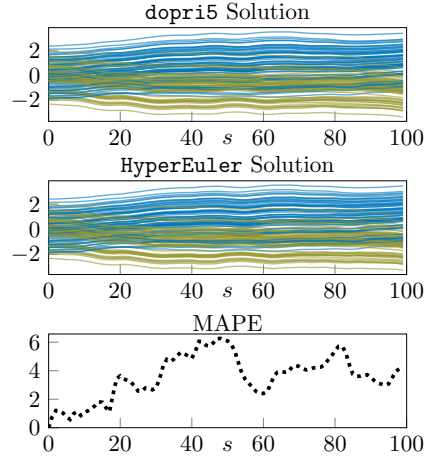


Figure 7: Through pure adversarial training, the Neural ODE dynamics  $f_{\theta(s)}$  learn to exploit *stiffness* to increase hypersolver errors.

## Broader Impact

Major application areas for continuous deep learning architectures so far have been generative modeling (Grathwohl et al., 2018) and forecasting, particularly in the context of patient medical data (Jia and Benson, 2019). While these models have an intrinsic interpretability advantages over discrete counterparts, it is important that future iterations preserve these properties in the search for greater scalability. Early adoption of the hypersolver paradigm would speed up widespread utilization of Neural ODEs in these domains, ultimately leading to positive impact in healthcare applications.

Accurate forecasting is at the foundation of system identification and control, two additional application areas set to be greatly impacted by continuous models. Unfortunately, theoretical guarantees of robustness in the worst-case scenario are challenging to construct for data-driven approaches. As these approaches are refined, they are also likely to negatively impact the employment market by accelerating job automation in critical areas.

## References

- S. Bai, J. Z. Kolter, and V. Koltun. Deep equilibrium models. In *Advances in Neural Information Processing Systems*, pages 688–699, 2019.
- G.-J. Both, S. Choudhury, P. Sens, and R. Kusters. Deepmod: Deep learning for model discovery in noisy data. *arXiv preprint arXiv:1904.09406*, 2019.
- P. G. Breen, C. N. Foley, T. Boekholt, and S. P. Zwart. Newton vs the machine: solving the chaotic three-body problem using deep neural networks. *arXiv preprint arXiv:1910.07291*, 2019.
- J. C. Butcher. *Numerical methods for ordinary differential equations*. John Wiley & Sons, 2016.
- J. Cash. Efficient numerical methods for the solution of stiff initial-value problems and differential algebraic equations. *Proceedings of the Royal Society of London. Series A: Mathematical, Physical and Engineering Sciences*, 459(2032):797–815, 2003.
- B. Chang, L. Meng, E. Haber, F. Tung, and D. Begert. Multi-level residual networks from dynamical systems view. *arXiv preprint arXiv:1710.10348*, 2017.
- T. Q. Chen, Y. Rubanova, J. Bettencourt, and D. K. Duvenaud. Neural ordinary differential equations. In *Advances in neural information processing systems*, pages 6571–6583, 2018.
- M. Cranmer, S. Greydanus, S. Hoyer, P. Battaglia, D. Spergel, and S. Ho. Lagrangian neural networks. *arXiv preprint arXiv:2003.04630*, 2020.
- T. Demeester. System identification with time-aware neural sequence models. *arXiv preprint arXiv:1911.09431*, 2019.
- J. Devlin, M.-W. Chang, K. Lee, and K. Toutanova. Bert: Pre-training of deep bidirectional transformers for language understanding. *arXiv preprint arXiv:1810.04805*, 2018.
- J. R. Dormand and P. J. Prince. A family of embedded runge-kutta formulae. *Journal of computational and applied mathematics*, 6(1):19–26, 1980.
- E. Dupont, A. Doucet, and Y. W. Teh. Augmented neural odes. In *Advances in Neural Information Processing Systems*, pages 3134–3144, 2019.
- J. Fang, C. Liu, T. Simos, and I. T. Famelis. Neural network solution of single-delay differential equations. *Mediterranean Journal of Mathematics*, 17(1):30, 2020.
- C. Finlay, J.-H. Jacobsen, L. Nurbekyan, and A. M. Oberman. How to train your neural ode. *arXiv preprint arXiv:2002.02798*, 2020.
- Y. Ganin, E. Ustinova, H. Ajakan, P. Germain, H. Larochelle, F. Laviolette, M. Marchand, and V. Lempitsky. Domain-adversarial training of neural networks. *The Journal of Machine Learning Research*, 17(1):2096–2030, 2016.
- I. Goodfellow, J. Pouget-Abadie, M. Mirza, B. Xu, D. Warde-Farley, S. Ozair, A. Courville, and Y. Bengio. Generative adversarial nets. In *Advances in neural information processing systems*, pages 2672–2680, 2014.
- W. Grathwohl, R. T. Chen, J. Bettencourt, I. Sutskever, and D. Duvenaud. Ffjord: Free-form continuous dynamics for scalable reversible generative models. *arXiv preprint arXiv:1810.01367*, 2018.

- S. Greydanus, M. Dzamba, and J. Yosinski. Hamiltonian neural networks. In *Advances in Neural Information Processing Systems*, pages 15353–15363, 2019.
- A. Gupta, R. Mendonca, Y. Liu, P. Abbeel, and S. Levine. Meta-reinforcement learning of structured exploration strategies. In *Advances in Neural Information Processing Systems*, pages 5302–5311, 2018.
- J. Han, A. Jentzen, and W. E. Solving high-dimensional partial differential equations using deep learning. *Proceedings of the National Academy of Sciences*, 115(34):8505–8510, 2018. ISSN 0027-8424.
- M. Hauser and A. Ray. Principles of riemannian geometry in neural networks. In *Advances in neural information processing systems*, pages 2807–2816, 2017.
- K. He, X. Zhang, S. Ren, and J. Sun. Delving deep into rectifiers: Surpassing human-level performance on imagenet classification. In *Proceedings of the IEEE international conference on computer vision*, pages 1026–1034, 2015.
- D. M. Hernandez and E. Bertschinger. Time-symmetric integration in astrophysics. *Monthly Notices of the Royal Astronomical Society*, 475(4):5570–5584, 2018.
- T. Hester. *TEXPLORE: Temporal Difference Reinforcement Learning for Robots and Time-Constrained Domains*. Springer, 2013.
- J. Howard and S. Ruder. Universal language model fine-tuning for text classification. *arXiv preprint arXiv:1801.06146*, 2018.
- J. Jia and A. R. Benson. Neural jump stochastic differential equations. In *Advances in Neural Information Processing Systems*, pages 9843–9854, 2019.
- Y. Khoo and L. Ying. Switchnet: a neural network model for forward and inverse scattering problems. *SIAM Journal on Scientific Computing*, 41(5):A3182–A3201, 2019.
- P. Kidger, J. Morrill, J. Foster, and T. Lyons. Neural controlled differential equations for irregular time series. *arXiv preprint arXiv:2005.08926*, 2020.
- I. Kobyzev, S. Prince, and M. A. Brubaker. Normalizing flows: Introduction and ideas. *arXiv preprint arXiv:1908.09257*, 2019.
- I. E. Lagaris, A. Likas, and D. I. Fotiadis. Artificial neural network methods in quantum mechanics. *Computer Physics Communications*, 104(1-3):1–14, 1997.
- I. E. Lagaris, A. Likas, and D. I. Fotiadis. Artificial neural networks for solving ordinary and partial differential equations. *IEEE transactions on neural networks*, 9(5):987–1000, 1998.
- S. Li and Y. Li. Nonlinearly activated neural network for solving time-varying complex sylvester equation. *IEEE transactions on cybernetics*, 44(8):1397–1407, 2013.
- X. Li-ying, W. Hui, and Z. Zhe-zhao. The algorithm of neural networks on the initial value problems in ordinary differential equations. In *2007 2nd IEEE Conference on Industrial Electronics and Applications*, pages 813–816. IEEE, 2007.
- Z. Long, Y. Lu, and B. Dong. Pde-net 2.0: Learning pdes from data with a numeric-symbolic hybrid deep network. *Journal of Computational Physics*, 399:108925, 2019.
- I. Loshchilov and F. Hutter. Decoupled weight decay regularization. *arXiv preprint arXiv:1711.05101*, 2017.
- Y. Lu, A. Zhong, Q. Li, and B. Dong. Beyond finite layer neural networks: Bridging deep architectures and numerical differential equations. *arXiv preprint arXiv:1710.10121*, 2017.
- M. Magill, F. Qureshi, and H. de Haan. Neural networks trained to solve differential equations learn general representations. In *Advances in Neural Information Processing Systems*, pages 4071–4081, 2018.
- S. Mall and S. Chakraverty. Comparison of artificial neural network architecture in solving ordinary differential equations. *Advances in Artificial Neural Systems*, 2013, 2013.
- S. Massaroli, M. Poli, M. Bin, J. Park, A. Yamashita, and H. Asama. Stable neural flows. *arXiv preprint arXiv:2003.08063*, 2020a.
- S. Massaroli, M. Poli, J. Park, A. Yamashita, and H. Asama. Dissecting neural odes. *arXiv preprint arXiv:2002.08071*, 2020b.

- R. I. McLachlan, G. Quispel, and G. S. Turner. Numerical integrators that preserve symmetries and reversing symmetries. *SIAM journal on numerical analysis*, 35(2):586–599, 1998.
- G. I. Parisi, R. Kemker, J. L. Part, C. Kanan, and S. Wermter. Continual lifelong learning with neural networks: A review. *Neural Networks*, 2019.
- A. Paszke, S. Gross, S. Chintala, G. Chanan, E. Yang, Z. DeVito, Z. Lin, A. Desmaison, L. Antiga, and A. Lerer. Automatic differentiation in pytorch. 2017.
- M. L. Piscopo, M. Spannowsky, and P. Waite. Solving differential equations with neural networks: applied to the calculation of cosmological phase transitions. *arXiv preprint arXiv:1902.05563*, 2019.
- M. Poli, S. Massaroli, J. Park, A. Yamashita, H. Asama, and J. Park. Graph neural ordinary differential equations. *arXiv preprint arXiv:1911.07532*, 2019.
- P. J. Prince and J. R. Dormand. High order embedded runge-kutta formulae. *Journal of Computational and Applied Mathematics*, 7(1):67–75, 1981.
- T. Qin, K. Wu, and D. Xiu. Data driven governing equations approximation using deep neural networks. *Journal of Computational Physics*, 395:620–635, 2019.
- M. Raissi. Deep hidden physics models: Deep learning of nonlinear partial differential equations. *The Journal of Machine Learning Research*, 19(1):932–955, 2018.
- M. Raissi, P. Perdikaris, and G. E. Karniadakis. Multistep neural networks for data-driven discovery of nonlinear dynamical systems. *arXiv preprint arXiv:1801.01236*, 2018.
- M. Raissi, P. Perdikaris, and G. E. Karniadakis. Physics-informed neural networks: A deep learning framework for solving forward and inverse problems involving nonlinear partial differential equations. *Journal of Computational Physics*, 378:686–707, 2019.
- F. Regazzoni, L. Dede, and A. Quarteroni. Machine learning for fast and reliable solution of time-dependent differential equations. *Journal of Computational Physics*, 397:108852, 2019.
- Y. Rubanova, T. Q. Chen, and D. K. Duvenaud. Latent ordinary differential equations for irregularly-sampled time series. In *Advances in Neural Information Processing Systems*, pages 5321–5331, 2019.
- C. Runge. Über die numerische auflösung von differentialgleichungen. *Mathematische Annalen*, 46(2):167–178, 1895.
- L. F. Shampine. *Numerical solution of ordinary differential equations*. Routledge, 2018.
- L. F. Shampine and C. W. Gear. A user’s view of solving stiff ordinary differential equations. *SIAM review*, 21(1):1–17, 1979.
- S. Sonoda and N. Murata. Double continuum limit of deep neural networks. In *ICML Workshop Principled Approaches to Deep Learning*, 2017.
- E. Weinan and B. Yu. The deep ritz method: a deep learning-based numerical algorithm for solving variational problems. *Communications in Mathematics and Statistics*, 6(1):1–12, 2018.
- N. Winovich, K. Ramani, and G. Lin. Convnpde-ug: Convolutional neural networks with quantified uncertainty for heterogeneous elliptic partial differential equations on varied domains. *Journal of Computational Physics*, 394:263–279, 2019.
- Z. Xing and L. McCue. Modeling ship equations of roll motion using neural networks. *Naval Engineers Journal*, 122(3):49–60, 2010.
- G. Yang, X. Huang, Z. Hao, M.-Y. Liu, S. Belongie, and B. Hariharan. Pointflow: 3d point cloud generation with continuous normalizing flows. In *Proceedings of the IEEE International Conference on Computer Vision*, pages 4541–4550, 2019.
- Ç. Yıldız, M. Heinonen, and H. Lähdesmäki. ODE2VAE: Deep generative second order odes with bayesian neural networks. *arXiv preprint arXiv:1905.10994*, 2019.
- H. Zhang, Z. Wang, and D. Liu. A comprehensive review of stability analysis of continuous-time recurrent neural networks. *IEEE Transactions on Neural Networks and Learning Systems*, 25(7):1229–1262, 2014.
- M. Zhu, B. Chang, and C. Fu. Convolutional neural networks combined with runge-kutta methods. *arXiv preprint arXiv:1802.08831*, 2018.

---

# Hypersolvers: Toward Fast Continuous–Depth Models

## *Supplementary Material*

---

### Table of Contents

<b>A Theoretical Results</b>	<b>12</b>
A.1 Proof of Theorem 1 . . . . .	12
A.2 Proof of Proposition 1 . . . . .	12
<b>B Further Discussion</b>	<b>13</b>
B.1 Software implementation . . . . .	13
B.2 Adversarial training . . . . .	13
<b>C Experimental Details</b>	<b>14</b>
C.1 Additional Experiments . . . . .	14
C.2 Image Classification . . . . .	14
C.3 Continuous Normalizing Flows . . . . .	16

---

## A Theoretical Results

### A.1 Proof of Theorem 1

**Theorem 1** (Hypersolver’s Local Truncation Error). *If  $g_\omega$  is a  $\mathcal{O}(\delta)$  approximator of  $\mathcal{R}$ , i.e.*

$$\forall k \in \mathbb{N}_{\leq K} \quad \|\mathcal{R}(s_k, \mathbf{z}(s_k), \mathbf{z}(s_{k+1})) - g_\theta(\epsilon, \mathbf{x}, s_k, \mathbf{z}(s_k))\|_2 \leq \mathcal{O}(\delta),$$

*then, the local truncation error  $e_k$  of the hypersolver is  $\mathcal{O}(\delta\epsilon^{p+1})$ .*

*Proof.* We can directly compute the local truncation error for the hypersolver as

$$e_k = \|z(s_{k+1}) - z(s_k) - \epsilon\psi(x, s_k, z(s_k)) - \epsilon^{p+1}g_\omega(\epsilon, x, s_k, z(s_k))\|_2$$

Thus,

$$\begin{aligned} e_k &= \epsilon^{p+1} \|\mathcal{R}(s_k, z(s_k), z(s_{k+1})) - g_\omega(\epsilon, x, s_k, z(s_k))\|_2 \\ &\leq \mathcal{O}(\delta\epsilon^{p+1}) \end{aligned}$$

□

### A.2 Proof of Proposition 1

**Proposition 1** (Vector field training sensitivity). *Let the model parameters  $\theta_t(s)$  be updated according to the gradient-based optimizer step*

$$\theta_{t+1}(s) = \theta_t(s) + \eta\Gamma(\nabla_{\theta(s)}\mathcal{L}_t), \quad \eta > 0$$

*to minimize a loss function  $\mathcal{L}_t$  and let  $f_{\theta_t(s)}$  be Lipschitz w.r.t.  $\theta(s)$ . Then,*

$$\forall \mathbf{z} \in \mathbb{R}^{n_z}, \quad \|\Delta f_{\theta_t}(\mathbf{x}, s, \mathbf{z})\|_2 \leq \eta L_{\theta(s)} \|\Gamma(\nabla_{\theta(s)}\mathcal{L})\|_2$$

*being  $L_\theta$  the Lipschitz constant.*

*Proof.* For the Lipschitz continuity of  $f_\theta$ , it holds

$$\forall \theta, \theta' \in \mathbb{R}^{n_\theta} \quad \|f_\theta - f_{\theta'}\|_2 \leq L_\theta \|\theta - \theta'\|_2$$

Thus,

$$\|\Delta f_{\theta_t}(x)\|_2 := \|f_{\theta_{t+1}}(x) - f_{\theta_t}(x)\|_2 \leq L_\theta \|\theta_{t+1} - \theta_t\|_2 = \eta L_\theta \|\Gamma(\nabla_\theta \mathcal{L})\|_2$$

□

## B Further Discussion

### B.1 Software implementation

We provide PyTorch (Paszke et al., 2017) code showcasing a minimal implementation of the *Euler hypersolver*.

```
class HyperEuler(nn.Module):
    def __init__(self, func, model):
        super().__init__()
        self.m = model # solver neural network
        self.f = func # neural ODE function

    def forward(self, ds, dx, x):
        """Estimate higher-order terms to compensate the truncation error at `x`"""
        ds = ds*torch.ones([*x.shape[:1], 1, *x.shape[2:]]).to(x)
        x = torch.cat([x, dx, ds], 1)
        x = self.m(x)
        return x

    def residual_trajectory(self, base_traj, s_span):
        """Recover residuals from a base trajectory"""
        ds = s_span[1] - s_span[0]
        fi = torch.cat(
            [self.f(s, base_traj[i])[None, :, :] for i, s in enumerate(s_span[:-1])])
        return (base_traj[1:] - base_traj[:-1] - ds*fi)/ds**2

    def _hypersolver_residuals(self, base_traj, s_span):
        """Calculate residual hypersolver predictions starting from a trajectory"""
        traj = []
        ds = s_span[1] - s_span[0]
        for i, s in enumerate(s_span):
            x = base_traj[i]
            dx = self.f(s, x).detach()
            res = self(ds, dx, x)
            traj.append(res[None])
        return torch.cat(traj)

    def trajectory(self, x, s_span):
        """Extrapolate a trajectory with span `s_span`"""
        traj = []
        ds = s_span[1] - s_span[0]
        for i, s in enumerate(s_span):
            dx = self.f(s, x).detach()
            traj.append(x[None])
            x = x + dx * ds + (ds**2)*self(ds, dx, x)
        return torch.cat(traj)
```

### B.2 Adversarial training

*Stiffness* in differential equations is an important problem of practical relevance as it often requires development of specialized solution methods (Shampine and Gear, 1979; Cash, 2003). While

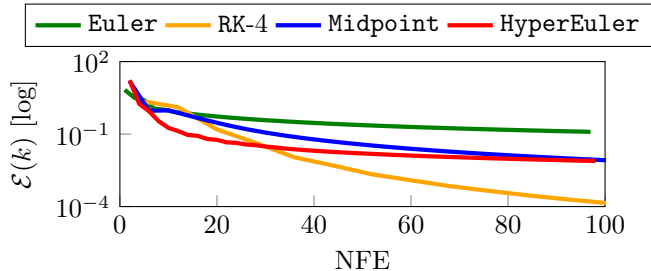


Figure 8: Pareto comparison of different solvers in the *trajectory tracking* task.

challenging to fully characterize, stiffness occurs when adaptive-step solvers require an extremely high number of solution steps to maintain the error below specified tolerances, in regions where the solution appears otherwise relatively smooth. In Fig. 7 we observe that the adversary Neural ODE  $f_\theta$  learns to exploit stiffness to increase the hypersolver error, thus teaching the model to handle dynamics of this type. Qualitatively, this phenomenon can be observed as the dynamics repeatedly manifest sudden variations, ultimately causing `dopri5` to decrease its step size and raise its required number of NFEs.

Inspired by the above proof of concept, further exploration of adversarial training strategies can thus aid in development of robust and general hypersolvers that can be applied to a wide variety of Neural ODE models, in both training as well as inference steps.

## C Experimental Details

**Computational resources** The experiments have been carried out on a machine equipped with a single NVIDIA Tesla V100 GPU and an eight-core Intel Xeon processor. In addition, we measured the *wall-clock* speedup against the *number of function evaluations* (NFEs) on three additional machines and found the results to be consistent across different setups.

### C.1 Additional Experiments

**Trajectory tracking** To evaluate the effectiveness of the trajectory fitting method, we consider a Galérkin Neural ODE (Massaroli et al., 2020b) tasked to tracking of a periodic signal  $\beta(s)$ . The Neural ODE is optimized with an integral loss of the type  $(\mathbf{z}(s) - \beta(s))^2$  in the integration domain  $S := [0, 1]$ . After the initial training of the model, we fit a three-layer HyperEuler of hidden dimensions 64, 64, 64 using a *trajectory fitting* approach.

Fig. 8 shows that the pareto efficiency in terms of global truncation error  $\mathcal{E}(k)$  is preserved when training with *trajectory fitting*. In the 10 - 25 NFE range, HyperEuler results more efficient than higher-order solvers such as midpoint and RK4.

### C.2 Image Classification

We report a detailed discussion on the hyperparameter and architectural choices made for the image classification experiments. Further experimental results are provided in Figures 9 and 10.

**Training hyperparameters** On MNIST, we optimized Neural ODEs for 20 epochs with batch size 32 utilizing the Adam optimizer with learning rate  $10^{-2}$  and a cosine annealing scheduler down to  $10^{-4}$  at the end of training. On CIFAR10, we utilized a similar strategy, with 20 epochs, batch size 16 and the same optimizer.

The HyperEuler hypersolver has been trained utilizing fitting the residuals of the *Dormand-Prince* solver (`dopri5`) (Dormand and Prince, 1980) with absolute and relative tolerances set to  $10^{-3}$ . We use the AdamW (Loshchilov and Hutter, 2017) optimizer with  $lr = 10^{-2}$  and a cosine annealing schedule down to  $5 * 10^{-4}$ .

The hypersolver training is subdivided into two phases, proceeding as follows. First, we stabilize the optimization by pretraining the hypersolver on the trajectories generated from a single batch for several iterations, usually 100. After this initial phase, the data batch is swapped every 10 iterations. This allows the hypersolver to generalize by having access to trajectories generated from different batches of the MNIST and CIFAR10 training sets.

We experimented with different numbers of iterations for hypersolver training. Convergence has been observed in as quickly as 5000 iterations, corresponding to *less than 3* epochs of the MNIST training dataset with batch size 32. In the main body of the paper we provide the much more conservative 20 epoch number. In practice, 20000 iterations (or 10 epochs) is sufficient to produce results comparable to the ones shown in Figures 9 and 10. A similar discussion applies to CIFAR10.

**Architectural details** In the following, we report PyTorch code defining the Neural ODE and hypersolver architectures in full. The code snippets are followed by a text description for accessibility. In MNIST, the architecture takes the form

```
f = nn.Sequential(nn.GroupNorm(3, 12),
                  nn.Conv2d(12, 64, 3, padding=1),
                  nn.Tanh(),
                  nn.Conv2d(64, 64, 3, padding=1),
                  nn.Tanh(),
                  nn.Conv2d(64, 12, 3, padding=1))

neuralDE = NeuralDE(f)

model = nn.Sequential(Augmenter(augment_func=nn.Conv2d(1, 11, 3, padding=1)),
                      neuralDE,
                      nn.Conv2d(12, 1, 3, padding=1),
                      nn.Flatten(),
                      nn.Linear(28*28, 10))
```

where the input-augmented layer (Massaroli et al., 2020b) Neural ODE  $f_\theta$  is defined as a sequence of convolutional layers of channel dimensions 12, 64, 12 and kernel size 3. The complete architecture is then composed of the above defined Neural ODE with a deconvolution layer, and a linear fully-connected layer to output the classification probabilities.

The HyperEuler architecture  $g_\omega$  is simpler and is composed of only a two-layer CNN with parametric-ReLU (PReLU) (He et al., 2015) activation. The input layer channel dimension is 25 whereas the input to  $f_\theta$ ,  $z(0)$  is only augmented to 12 channels. This is because  $g_\omega$  takes a concatenation of  $z, f_\theta(z), s$  which yields  $12 + 12 + 1$  channels.

```
g = nn.Sequential(nn.Conv2d(25, 32, 3, padding=1),
                  nn.PReLU(32),
                  nn.Conv2d(32, 12, 3, padding=1))

solver = CNNHypersolver(f, g)
```

For the CIFAR10 experiments, on the other hand,  $f_\theta$  and the complete architectures are defined as

```
f = nn.Sequential(DepthCat(1),
                  nn.Conv2d(9, 64, 3, padding=1),
                  nn.BatchNorm2d(64),
                  nn.Tanh(),
                  DepthCat(1),
                  nn.Conv2d(65, 64, 3, padding=1),
                  nn.BatchNorm2d(64),
                  nn.Tanh(),
                  nn.Conv2d(64, 8, 3, padding=1))
```

```

neuralDE = NeuralDE(f)

model = nn.Sequential(Augmenter(augment_func=nn.Conv2d(3, 5, 3, padding=1)),
                      nn.BatchNorm2d(8),
                      neuralDE,
                      nn.Conv2d(8, 1, 3, padding=1),
                      nn.Flatten(),
                      nn.Linear(32*32, 10))

```

In this case, we consider  $f_{\theta(s)}$  to be a depth-varying dynamics utilizing depth-concatenation as proposed in (Chen et al., 2018). The tt HyperEuler architecture is

```

g = nn.Sequential(nn.Conv2d(17, 64, 5, padding=2),
                  nn.PReLU(64),
                  nn.Conv2d(64, 32, 5, padding=2),
                  nn.PReLU(32),
                  nn.Conv2d(32, 8, 3, padding=1))

solver = CNNHypersolver(f, g)

```

It should be noted that the focus of these experiments has not been optimizing  $f_{\theta}$  for task-performance. Indeed, we observed that HyperEuler obtains similar results to those shown in the main body of the paper and in Figures 9 and 10 across a variety of different  $f_{\theta}$ .

**Results** To highlight the efficacy of hypersolvers, we utilize the following metrics

- *Absolute error* of the numerical solution at different solution mesh points. (Figures 3, 4, 9, 10). These results provide qualitative proof of the higher solution accuracy of hypersolvers across different types of data samples.
- *Mean absolute percentage error* (MAPE) of the terminal solution at mesh point  $k = K - 1$  (Figure 5). Pareto efficiency of hypersolvers numerical solutions.
- *Average test accuracy decrement* (Figure 3). We measure the average (across batches) accuracy lost by a transition away from `dopri5`. The objective has been to show that outside of solution accuracy, hypersolvers offer pareto efficiency over other solvers in terms of task-specific metrics.

We provide additional results in Figures 9 and 10 to further contextualize the hypersolver performance with different types of data samples. Interestingly, CIFAR10 Neural ODE dynamics are easier to learn for hypersolvers. This is because CIFAR10 data-samples provide useful dynamics information in the entire image, including the background, whereas MNIST digits contain little information as the background is uniform. As a result, the numerical hypersolver solution preserves high-accuracy for all pixels, yielding the red patches observed in 10

### C.3 Continuous Normalizing Flows

We optimize *continuous normalizing flows* (CNF) (Chen et al., 2018) on density estimation tasks, closely following the setup of (Grathwohl et al., 2018). For a complete reference on normalizing flows we refer to (Kobyzev et al., 2019).

In particular, the training for the two-dimensional tasks is carried out for 1500 iterations with an Adam optimizer set to constant learning rate  $10^{-3}$ . The CNF is constructed with a three-layer MLP of hidden dimensions 128, 128, 128 and the corresponding ODE is solved with `dopri5` with absolute and relative tolerances set to  $10^{-5}$  for an accurate forward propagation of the log-density change (Chen et al., 2018). We consider several standard two-dimensional densities following (Grathwohl et al., 2018), namely `pinwheel`, `rings`, `checkerboard` and a modified, more challenging `circles` where the annuli are connected by three curves.

After this initial step, we train an *Heun hypersolver* for 30000 iterations of residual fitting on *backward* trajectories (sampling regime) utilizing a similar strategy as discussed in the previous subsection. Namely, we leverage *AdamW* (Loshchilov and Hutter, 2017) with  $lr = 10^{-3}$ , weight decay  $10^{-6}$  and a two-stage training where the data-sample generating the residuals is switched after every 100 iterations.

**Depth-reversibility** The training and inference of CNF heavily relies on the reversability property of differential equations (strictly related to the uniqueness of ODE solutions), namely that there exists a symmetry between trajectories solved forward and backward in the detph domain.

In particular, the density estimation step of CNF is carried out by integrating the ODE forward in  $S$  while the sampling takes place solving the model backward. Therefore, it is natural to require some reversability properties of the numerical solver practically used to solve the IVP. There exists a whole line of work studying whether or not a numerical integrator preserves different symmetries, including reversability (McLachlan et al., 1998; Hernandez and Bertschinger, 2018). In this context, the Euler method results to be not reversible, and can be shown to be accumulating error when reversing the integration direction. Thus, the HyperEuler would not be a good choice when it comes to CNF and, instead, we would like to look for a reversible hypersolver “base”. Our choice has been the Heun method (or RK(2)), which is the lowest-order solver enjoying theoretical guarantees on depth-reversibility (Hernandez and Bertschinger, 2018).

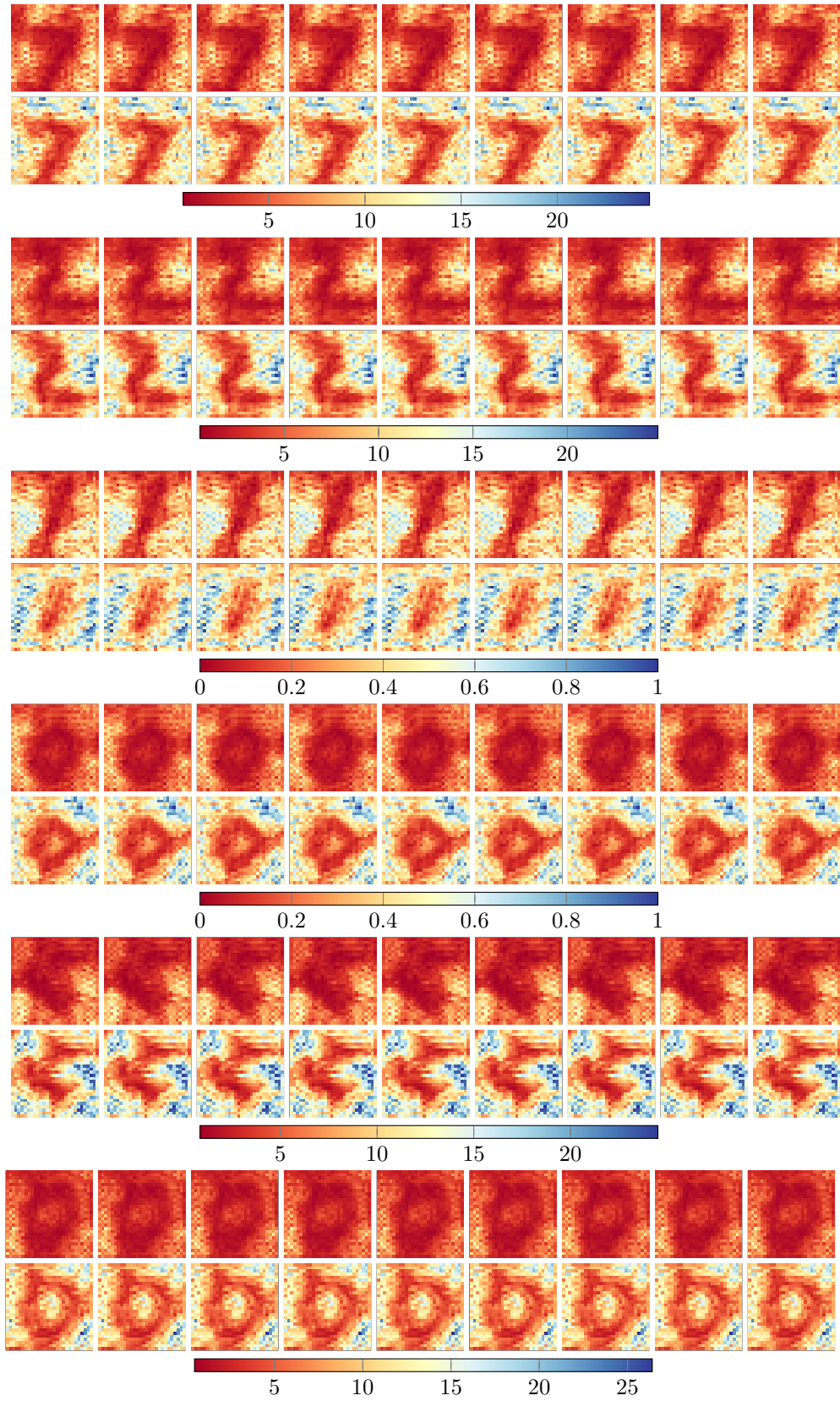


Figure 9: Absolute integration error propagation through the depth domain of the HyperEuler (above) and Euler (below) methods on MNIST data.



Figure 10: Absolute integration error propagation through the depth domain of the HyperEuler (above) and Euler (below) methods on CIFAR10 data.